Magnetic nanoparticles with inhomogeneous and core/shell structures

Author: Pol Adillon Albero
Dpt. Física de la Matèria Condensada, Facultat de Física,
*Universitat de Barcelona, Av. Diagonal 645, 08028 Barcelona, Spain.**

Advisor: Òscar Iglesias Clotas

Abstract: In this work, we present the results of atomistic-level simulations of the magnetic properties of individual magnetic nanoparticles (NP) with a variety of morphologies and compositions. For this purpose, we have set up a computer code that uses the Monte Carlo method to simulate Heisenberg classical spins residing on the nodes of different kinds of 3D lattices, including exchange interactions between them, magnetocrystalline uniaxial anisotropy, and the effect of an external magnetic field. Finite-size and surface effects on the equilibrium magnetic configurations and hysteresis loops of single-phase NP have been studied varying the shape and surface anisotropy of the NP. We also present results of the reversal mechanisms of NP with (ferromagnetic (FM)/antiferromagnetic(AF)) core/shell morphology, showing that they exhibit the exchange bias (EB) phenomenon in the hysteresis loops after a field cooling (FC) process and unveiling the microscopic origin of this phenomenon. Finally, the possibility of observing EB effects in NP with inverted core(AF)/shell(FM) structure will be explored and their magnetic properties compared to those with the conventional morphology.

I. INTRODUCTION

Nanoparticles, especially magnetic ones, are gaining research interest in the last decades [1]. This is mainly due to their promising applications in various technological applications, such as magnetic recording, magnetic sensors, permanent magnets, quantum computing, and spintronics [2] as well as biomedical and environmental applications such as drug delivery, magnetic resonance imaging or water treatment [3]. In particular, let us mention two examples: a) the recent proposal to use magnetic NP in cancer treatment techniques as hyperthermia, a noninvasive and selective method whereby NP release heat when an external variable magnetic field is applied, killing the cancerous cells [4], b) the observation of exchange bias effects in NP with core/shell structures that can be used to beat the superparamagnetic limit in magnetic recording [5]. A great improvement in manufacturing procedures has back up the increasing attention in NP. We can now synthesize NP with narrow size distributions which range from few nanometers up to a hundred nanometers, and with specific shapes, such as cubes, spheres, hollow spheres, or tetrahedrons. Several chemical and physical routes can be used to fine-tune their material compositions and their crystallographic structure.

In the present work, we have set up a computer code that will allow simulating the magnetic properties of NP taking into account the shape, size, composition, and different morphologies. The results of the simulations will help us to address some important issues that might be relevant for the applications of NP to the previously mentioned fields. We do not aim to study a particular material but to understand how changing different parameters of the NP might affect its magnetic properties.

Finite-size and surface effects can strongly affect the magnetic properties of materials as compared to their bulk counterpart when reducing the size of a magnetic element to the nanoscale [8]. The breaking of the crystal symmetry and reduced coordination at the surface spins leads to roughness and magnetic disorder at the NP surface, resulting in changes in the magnetic anisotropy, both in magnitude and direction. Therefore, we will address these effects in the first part of our work (Sec. III). Next, we will study how the magnetization reversal mechanism of monophasic FM NP changes when considering different NP shapes and sizes, even in the monodomain limit.

In the second part (Sec. IV), we will focus on a typical morphology such as NP with core/shell structure. A common way to create it is by letting the metallic core get oxidized so a thin layer of oxide is placed surrounding it. Some of the most common compounds used have Fe at the core and a shell of maghemite, Fe_2O_3 or magnetite, Fe_3O_4[both ferrimagnetic (FiM)] or Co at the core with an outer layer of AF CoO or Co_3O_4 (FiM). The observation of EB was first reported in this kind of NP [6] so that we will start studying the parameters that influence this phenomenon and its origin in this more usual structure. We will finish showing that EB can also be found in fully oxidized core/shell inverted NP such as the ones an AF such MnO at the core and a FiM shell Mn_3O_4 reported in [7].

II. MODEL

Most of the NP considered here will be spheres with a total radius R cut from a cubic lattice with Heisenberg classical spins placed at the nodes. However, the code

*Electronic address: pol.adillon@gmail.com

has also the possibility to generate fcc, bcc and spinel lattices that will not be considered here. In core/shell structures, we have distinguished three parts: the core, the shell, and the interface. This last one includes the spins that have neighbors both in the core and the shell. The thickness of the shell is R_S. The spins are deemed to be interacting at first neighbors and under an external magnetic field H. Hence, we can write the Hamiltonian of the system as follows [9]:

$$\begin{aligned}\mathcal{H}/k_{\rm B} = &- J_{\rm C} \sum_{\langle i,j\rangle\in {\rm C}} \vec{S}_i\cdot\vec{S}_j - J_{\rm S} \sum_{\langle i,j\rangle\in {\rm Sh}} \vec{S}_i\cdot\vec{S}_j \\ &- J_{\rm Int} \sum_{\langle i\in {\rm C}, j\in {\rm Sh}\rangle} \vec{S}_i\cdot\vec{S}_j - K_{\rm C}\sum_{i\in {\rm C}} (S_i^z)^2 \\ &- K_{\rm S}\sum_{i\in {\rm Sh}} (S_i^z)^2 - \sum_{i=1}^{N} \vec{h}\cdot\vec{S}_i \ ,\end{aligned} \tag{1}$$

where $k_{\rm B}$ is the Boltzmann constant and, therefore all material constants, including the magnetic field are given in temperature units (K).

The first three terms stand for the interactions of near-neighbors spins of each region. J determines the coupling between a pair of spins. If $J > 0$, we will have a FM material, favoring parallel alignment, whereas $J < 0$, the material will be AF, favoring antiparallel spin alignment. In FiM spinel oxides, the magnetic ions in different sublattices tend to be oriented antiparallel to each other and the total magnetic moment is not fully compensated. Therefore, in a simplified approach, they can be modeled as FM. Most of the results will be shown for spherical NP with R of 12 unit cells of dimension a, and a shell of thickness $R_{\rm S} = 3a$. We have set as a reference value $J_c = 1$ K, which gives a FM ordering temperature $T_C \simeq 2.9$ K and fixed $J_s = -0.5$ K, as in most of the considered AF materials the Neél temperature $T_N < T_C$. $J_{\rm Int}$ will be allowed to vary in magnitude and sign.

The fourth and fifth terms correspond to the anisotropy, uniaxial along the z-axis unless stated otherwise. The anisotropy constants, $K_{\rm C}$ and $K_{\rm S}$, have been also rescaled with respect to real values $k_{\rm C}$ and $k_{\rm S}$, that have units of energy per unit volume or surface respectively, in the following way:

$$K_{\rm C} = \frac{k_{\rm C}V}{N_{\rm C}}, \quad K_{\rm S} = \frac{k_{\rm S}S}{N_{\rm S}} \tag{2}$$

where V is the volume of the core and S is the surface of the NP. With lower K the spins will be reversed easily under the application of an external field. The last term, the Zeeman energy, is the coupling between the spins and an external magnetic field H that verifies: $h = \mu H/k_{\rm B}$, where μ is the magnetic moment of the spin.

The code is based on the Monte Carlo method using the Metropolis algorithm. The main idea of this method is to change spins and look at how the energy varies. As we are working with Heisenberg spins, we have not sorted the new spin direction at random, when proposing it. Instead, we have generated it uniformly inside a cone of a given small maximum aperture around the old spin direction, so that anisotropy energy barriers are sampled correctly.

When presenting hysteresis loops, we will plot the magnetization component along the external field direction considered as the z-axis. In core/shell NP, magnetizations will be normalized to the number of spins in the region under consideration and will be denoted as follows: $M_{\rm C}$, $M_{\rm S}$, $M_{\rm Int}$ for the core, shell and interface regions and $M_{\text{Int-S}}$, $M_{\text{Int-C}}$ for the core and surface interfacial spins contributions, respectively. When considering EB effects in core/shell NP, we will simulate hysteresis loops performed after two protocols: a) zero-field cooled (ZFC) conditions, starting from a disordered configuration in zero-field and applying a field towards saturation, b) field cooling (FC) from a high temperature above T_C in the presence of an external field and then perform then cycling the field. The resulting loops can be characterized by: 1) the coercive field, which is a measure of the magnetic field needed to reduce the magnetization to zero; 2) the EB field, which characterizes the displacement of the loop center of the hysteresis loop along the field axis. They are defined as:

$$h_{\rm C} = (h_{\rm C}^+ - h_{\rm C}^-)/2 \ , h_{\rm eb} = (h_{\rm C}^+ + h_{\rm C}^-)/2 \tag{3}$$

where $h_{\rm C}^+$, $h_{\rm C}^-$ are the coercive fields at the increasing and decreasing field branches.

III. RESULTS FOR SINGLE PHASE NP

FM particles: uniaxial and radial shell anisotropy. Let us start considering a FM nanoparticle of $R = 12a$, and $J = 1$. In a first macrospin approximation, the anisotropy can be considered to be uniaxial along the same direction z that the external magnetic field is applied. A more accurate picture of a real NP should take into account that spins on the external surface of the NP, those with coordination numbers lower than the bulk material (6 for the sc lattice), will have a different crystalline field than those in the NP core. This can be incorporated [1] by assigning radial anisotropy direction (Neél anisotropy) to the outer layer of spins that will tend to misalign them from those in the core.

For the uniaxial anisotropy, we have chosen $K = 0.1$ (red, Fig. 1), and $K_{\rm rad} = 0.1$ (green, Fig. 1) and $K_{\rm rad} = 1$ (blue, Fig. 1) for the radial surface anisotropy. Let us see how this hedgehog-like configuration affects the hysteresis loop of the total magnetization.

In Fig. 1, we notice that introducing a radial anisotropy in the surface reduces the width of the hysteresis loop, h_C (Eq. 3). That is because, as many spins of the surface are already pointing in the opposite direction of H, it is easier to change $M_{\rm Total}$. We also lose magnetization (flat parts of the plot) caused by the disorder of the shell. With larger H we reach the magnetization of the uniaxial anisotropy particle (blue line matches red

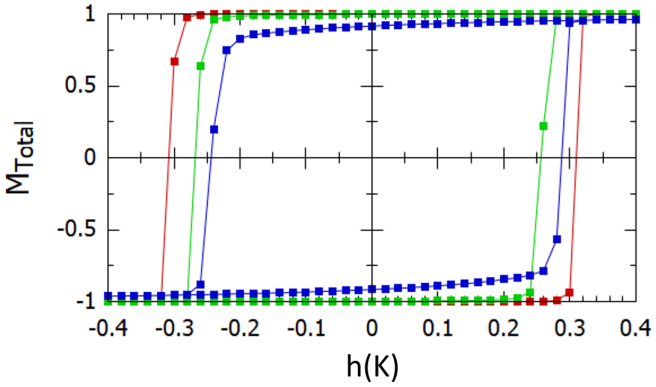

FIG. 1: Hysteresis loops with ZFC for M_{Total} for a particle with $R = 12a$, $J = 1$. (Red) Uniaxial anisotropy $K = 0.1$. (Green) Radial surface anisotropy with $K_{\text{rad}} = 0.1$. (Blue) Radial surface anisotropy with $K_{\text{rad}} = 1$.

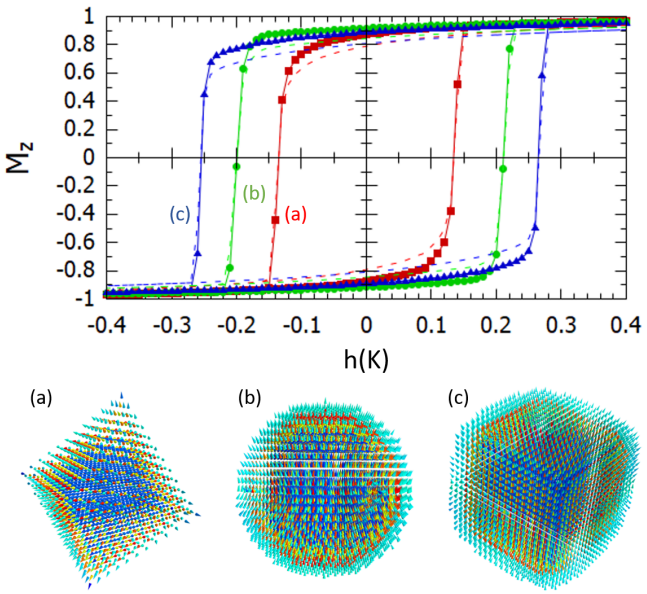

FIG. 2: Main panel: hysteresis loops after ZFC process for M_{Total} (symbols) and M_{S} (dashed lines) for single phase FM NP with $R = 12a$ but different shapes correponding to Eq. 4: (a) $p = \frac{1}{2}$; (b) $p = 1$; (c) $p = \frac{5}{2}$. Lower panels show snapshots of the equilibrium magnetic configurations in zero field for the three shapes. In all cases, $J_{\text{C}} = 1$, $J_{\text{S}} = 1$, $K_{\text{C}} = 0.1$ $K_{\text{S}} = 1$ and radial surface anisotropy have been included.

line). With larger K_{rad} we need stronger H to brush the surface spins toward the direction of the external field, this makes these effects of the radial anisotropy more noticeable when K_{rad} is bigger.

NP shape effects. Inspired by recent experimental studies [10], we included in our program the possibility to tune the shape of the NP continuously from octahedral ($p = 1/2$) to cubic ($p \to \infty$) by cutting the spin lattice according to the region that verifies:

$$x^{2p} + y^{2p} + z^{2p} < R^{2p} \tag{4}$$

To study the effect of the shape of the NP on its hysteresis loop, we have considered three core-shell particles with $p = \frac{1}{2}$, $p = 1$ and $p = \frac{5}{2}$. All three NPs have $R = 12a$, $J_{\text{C}} = 1$, $J_{\text{S}} = 1$, $J_{\text{Int}} = 1$, $K_{\text{C}} = 0.1$ and $K_{\text{S}} = 1$ and a radial anisotropy in the outside layer $K_{\text{rad}} = 1$.

The snapshots of the equilibrium magnetic configurations attained at low temperatures in Fig. 2 (lower panels), we can see the formation of nonuniform structures in form of different magnetic ordering at the outer shells of spins due to surface anisotropy that is propagated inside the core region inducing departures from its easy axis that depend on the NP shape. These effects are more pronounced for spheres and octahedrons than for cubes and, as a consequence, they will influence the magnetization reversal mechanism as can be seen in the simulated hysteresis loops shown in Fig. 2. We notice that the total magnetization reverses in a non-uniform way as indicated by the non-squared shape of the loops which is more pronounced for non-spherical shapes. The reversal process is dominated by the surface contribution M_{S} (dashed lines) that, together with the geometry of the NP, is also responsible for the observed increase in the coercive field as the shape approaches a cube. Interestingly, our results show that the area of the loops (related to the heat power released in hyperthermia experiments) can be tuned by changing the shape, being maximized for cubic NP, in agreement with previously reported results [4].

IV. RESULTS FOR CORE/SHELL NP

Effect of the shell. We want to study core/shell NP, so first, we should see which are the effects of wrapping a FM single-phase NP with an AF shell. For this purpose, we consider a single phase NP with $R = 10a$, $J = 1$ and $K = 0.1$, and two core/shell NP with $R = 12a$, $R_{\text{S}} = 3a$, $J_{\text{C}} = 1$, $J_{\text{S}} = -0.5$ and $K_{\text{C}} = 0.1$. One core-shell NP has $K_{\text{S}} = 0.1$ and the other $K_{\text{S}} = 1$. Two signs for the interfacial exchange coupling cases have been considered: $J_{\text{Int}} > 0$ (Fig. 3.a) and $J_{\text{Int}} < 0$ (Fig. 3.b).

Fig. 3 shows how a shell with $J_{\text{S}} < 0$ reduces h_{C}. This is mainly because the spins of the core, especially the interface ones, reproduce the anti-parallel pattern of the shell spins. Then, it is easier for the external field H to flip the spins since there are fewer spins to be flipped into the direction of H.

Another noticeable point is that h_{C} is lower if K_{S} is larger. As long as the core and the shell are connected ($J_{\text{int}} \neq 0$) the shell will also mimic the parallel pattern of the core. But, with larger anisotropy K_{S}, the spins of the shell are less likely to change under the variation of

H or vary along the core spins. Fig. 3.a.2 and Fig. 3.b.2 shows that: the height of the hysteresis loop for $M_{\text{Int-S}}$ decreases as K_S increases. Hence, with bigger K_S we get less h_C because again, there are fewer spins to change.

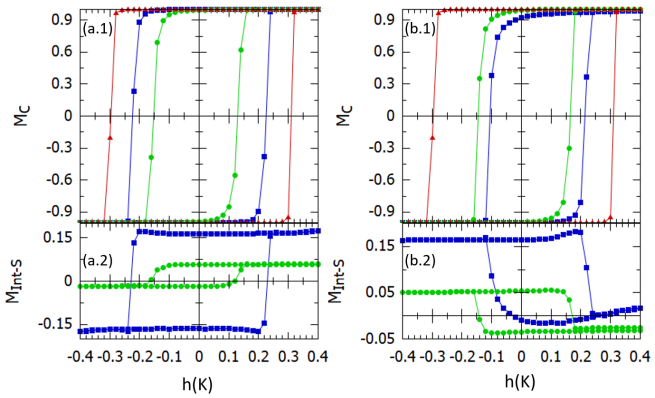

FIG. 3: Hysteresis loops with ZFC for M_C and $M_{\text{Int-S}}$. The red triangles are a not shell particle with $R = 10a$, $J = 1$ and $K = 0.1$. For green dots and blue squares we have got a core-shell particle of $R = 12a$, $J_C = 1$, $J_S = -0.5$ and $K_C = 0.1$, being green dots $K_S = 1$ and blue squares $K_S = 0.1$. Left and right panels differ by J_{Int}: (a) $J_{\text{Int}} = 0.25$ and (b) $J_{\text{Int}} = -0.25$.

For $J_{\text{Int}} = -0.25$, Fig. 3.b, we can see a little EB to the right for $K_S = 0.1$ (blue squares). This is a reflection of the behavior of $M_{\text{Int-S}}$, Fig. 3.b.2. In this case, $M_{\text{Int-S}}$ stays above 0 almost for each H. This asymmetry causes the shift toward the right we see in the hysteresis loop, and it might come from the initial configuration of spins.

Hysteresis loops after FC in core/shell NP. The EB phenomenon typically appears when we have a FM or FiM core, surrendered by an AF shell. When cooling the NP, the interface shell spins will set parallel ($J_{\text{Int}} > 0$) or opposite ($J_{\text{Int}} < 0$) to interface core spins, and if K_S is greater than K_C, the spins of the shell will freeze in that direction. When the H is reversed, the core will do so, but it will feel a magnetic field h_{eb} caused by the frozen interface shell spins that remain unchanged. h_{eb} will be always in the same direction, as shell spins are fixed, so sometimes its effect will be added to H or will be in the opposite direction. This process produces a shift in the hysteresis loop, i.e. EB.

This can be easily seen in Fig. 4. In both panels, (a) and (b), we have an EB toward the left when a FC is realized before the hysteresis loop (red squares). When we have an EB, the interfaces spins are not symmetric with respect to the horizontal axis: (a.2) $M_{\text{Int-S}} \approx 0,15$ (b.2) $M_{\text{Int-S}} \approx -0,15$.

Effect of J_{int} on the FC hysteresis loops. We have already seen how EB and h_C depend on the value of J_{int}. We can go one step further and try to describe this dependence more deeply. To do this, we have used the same NP as in Fig.4 (red squares) ($R = 12a$, $J_C = 1$, $J_S = -0.5$, $K_C = 0.1$, $K_S = 1$) for different values of J_{int}. Fig. 5 shows the results found using equations 3.

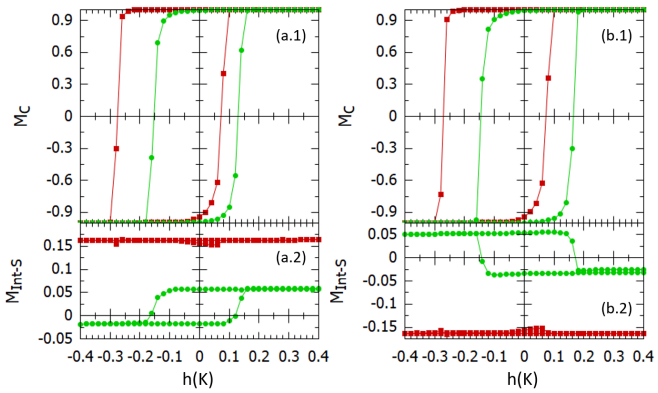

FIG. 4: Hysteresis loops for M_C and $M_{\text{Int-S}}$. We have core-shell particles with $R = 12a$, $J_C = 1$, $J_S = -0.5$, $K_C = 0.1$ and $K_S = 1$. The red squares represent hysteresis cycle with FC of an external magnetic field $h = 0.4$. The green dots represent hysteresis cycle whit ZFC. Left and right panels differ by J_{Int}: (a) $J_{\text{Int}} = 0.25$ and (b) $J_{\text{Int}} = -0.25$.

We can see that by increasing $|J_{\text{int}}|$ we reduce h_C. $K_S > K_C$ so the shell spins will be more rigid than the core spins. With bigger coupling between the two regions, the core will replicate easily the anti-parallel pattern of the shell, hence fewer spins will need to be changed when varying the value of the external magnetic field, that is less H to magnetize the NP, so a smaller h_C. In terms of EB, while the shell is frozen, h_{eb} in module is larger with greater interaction between the two regions. This coincides with the case of independent core and shell, $J_{\text{Int}} = 0$, where the shift of the hysteresis loop is zero, since the shell spins cannot influence the core spins.

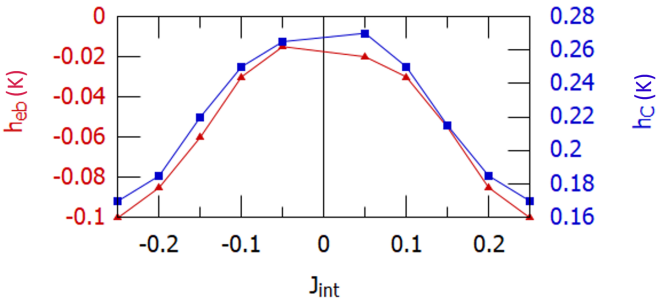

FIG. 5: (Red triangles) Exchange bias, h_{eb} calculated with Eq. 3, as a function of J_{Int}. (Blue squares) width of the hysteresis loop, h_C calculated with Eq. 3, as a function of J_{Int}.

Inverted core/shell NP. We call inverted nanoparticle the NP with an AF core and a FM shell. This is because Fe, Co, Mn and Ni are FM and are normally in the core. This is not just a theoretical exercise as this type of particles exist and is been synthesized in labs [6]. Fig. 6.a shows the spin configuration at $T = 0.01$ after

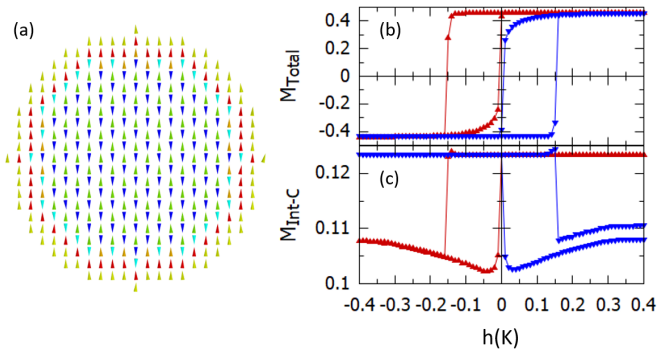

FIG. 6: (a) Slice of the inverted NP that shows the spin configuration at $T = 0.01$ after a FC. $R = 12a$, $J_C = -1$, $J_S = 0.5$, $J_{Int} = 0.25$, $K_C = 1$ and $K_S = 0.1$. Panels on the right show the M_{Total} (b) and $M_{Int\text{-}S}$ (c) contributions to the hysteresis loops after a FC in a field $h = 0.4$. Blue triangles: $J_{Int} = 0.25$. Red triangles: $J_{Int} = -0.25$.

a FC. We can see the AF core with anti-parallel spins and the FM shell with parallel spins. We have considered two inverted particles with parameters: $R = 12a$, $J_C = -1$, $J_S = 0.5$, $K_C = 1$ and $K_S = 0.1$. One of them has $J_{Int} = 0.25$ (blue triangles in Fig. 6), the other one $J_{Int} = -0.25$ (red triangles Fig. 6)

A considerable shift is seen in Fig. 6 for both NPs, but in opposite directions. This is mainly caused by the big influence of the frozen core spins over the thin shell. By taking a closer look, we can notice that the decreasing field branch and the increasing field branch of the M_{Total} are not symmetrical, Fig. 6.b. For instance, in the $J_{Int} = 0.25$ NP (blue triangles Fig. 6.b and Fig. 6.c) the decreasing field branch ($M_{Total} > 0$) is smother than the increasing field branch that is steeper. The explanation of this phenomena can be found by looking into different configurations of the NP during the hysteresis loop. The spins don't change in unison, so some regions will change before others. This may vary in each branch causing this asymmetry.

V. CONCLUSIONS

We have developed a computer code to simulate, by Monte Carlo methods, the magnetic properties of individual NP at the atomistic level, with different shapes and morphologies. Several examples demonstrating the capabilities of the code have been presented. Regarding single-phase FM NP, we have studied the influence of surface Neél anisotropy showing that it is responsible for the reduction in magnetization as compared to the ideal uniaxial case and a reduction in the coercive field. We have reported an increase in the hysteresis loop area and h_c for the cubic case when comparing the hysteresis loops of NP with different shapes, which is in agreement with hyperthermia measurements. In NP with core/shell morphology, we have traced back the origin of the observed shifted loops after FC to the existence of a net uncompensated moment of the interfacial shell spins that is responsible for the EB effect due to the coupling of the AF shell to the FM core. Finally, we have considered also NP with inverted core/shell morphology, demonstrating that considerable EB effects can also be observed in this case with loops that can be shifted from negative to positive along the field axis by tuning the sign of the exchange coupling at the interface. In future work, we would like to extend the simulations to more realistic lattices (oxides and FiM materials), to include real units for atomic moments and fields, and to consider cubic anisotropies that would allow comparing better with experimental results. Inclusion of interatomic dipolar interactions should also be possible by adding a specific module to compute them, this would allow studying the formation of magnetic domains in bigger NP.

Acknowledgments: I would like to thank my advisor Òscar Iglesias for all the knowledge he has shared with me and his patience during the long Zoom calls to set up the code and discuss simulation results. Also CSUC for computational resources.

[1] Ò. Iglesias, H. Kachkachi, Ch. 1, p. 3-38 in *New Trends in Nanoparticle Magnetism*, (Springer, Cham, 2021).
[2] Kannan M. Krishnan *Fundamentals and Applications of Magnetic Materials*, (Oxford Univ. Press, 2016).
[3] R. L. Stamps et al. J. Phys. D: Appl. Phys. **47**, 333001 (2014).
[4] C. Martínez- Boubeta et al. Scientific Reports **3**, 1652 (2013).
[5] V. Skumryev et al. Nature **423**, 850 (2003).
[6] J. Nogués, I.K. Schuller, J. Magn. Magn. Mater. **192**, 203 (1999).
[7] G. Salazar-Álvarez et al., J. Am. Chem. Soc. **129**, 9102 (2007); A. López-Ortega et al., J. Am. Chem. Soc. **132**, 9398 (2010).
[8] A. Labarta, X. Batlle, Ò. Iglesias, Ch. p. 105-140 in *Surface Effects in Magnetic Nanoparticles*, (Springer, Boston, 2005).
[9] Ò. Iglesias et al., Phys. Rev. B **72**, 212401 (2005); J. Nanosci. Nanotecn. **8**, 2761 (2008).
[10] D. Dresen et al. ChemRxiv 20210520 (unp. preprint) (2021); B. Rivas-Murias et al. Chem. Mater. **32**, 10435 (2020).